A dielectric slit die for in-line monitoring of polymer compounding

Anthony J. Bur,[a] Steven C. Roth, and Yu-Hsin Lee
National Institute of Standards and Technology, Gaithersburg, Maryland 20899-8542

Michael McBrearty
Chemical ElectroPhysics, Hockessin, Delaware 19707

(Received 28 October 2003; accepted 15 January 2004; published 16 March 2004)

The dielectric slit die is an instrument that is designed to measure electrical, rheological, ultrasonics, optical, and other properties of a flowing liquid. In one application, it is connected to the exit of an extruder, pump or mixing machine that passes liquefied material such as molten plastic, solvents, slurries, colloidal suspensions, and foodstuffs into the sensing region of the slit-shaped die. Dielectric sensing is the primary element of the slit die, but in addition to the dielectric sensor, the die contains other sensing devices such as pressure, optical fiber, and ultrasonic sensors that simultaneously yield an array of materials property data. The slit die has a flexible design that permits interchangeability among sensors and sensor positions. The design also allows for the placement of additional sensors and instrumentation ports that expand the potential data package obtained. To demonstrate sensor operation, we present data from the extrusion and compounding of a polymer/clay nanocomposite. An analysis of the dielectric data involves a nonlinear fitting procedure that takes into account effects due to electrode polarization and dc conductivity. Light transmission through a filled polymer is analyzed in terms of a Beer's law attenuation coefficient. [DOI: 10.1063/1.1667256]

I. INTRODUCTION

In previous work we described a first generation dielectric sensor that we used for in-line monitoring of polymer compounding.[1,2] That sensor consists of a ceramic ring that has interdigitating electrodes deposited on its inside surface. As an extruded resin or liquid flows through the ring, its dielectric properties are monitored by a fringing electric field that extends into the liquid. Using this sensor, we measured dielectric properties of resin melts compounded with inorganic fillers. The sensor provided access to parameter space that has been investigated rarely, i.e., the dielectric properties of polymer melts. While the literature abounds with dielectric measurements on polymers in the solid state,[3] measurements on the melt state are not attempted because of problems due to resin degradation and due to potential damage to the dielectric cell from resin melt and decomposition.[4] We avoid these problems by making measurements during steady-state extrusion whereby the polymer is continuously replenished in the sensing region of the dielectric cell.

The interdigitating electrode design has the advantage that the sensor is one-sided and does not involve sensing across the full dimension of the flow stream. On the other hand, it has the disadvantage that the sensing electric field is confined to the near surface region. For a 12.7 mm diameter cell, that we previously described, with interdigitating electrodes that are separated by 0.33 mm, the field extends only 0.4 mm into the resin melt. Consequently, only 10% of the cross section of resin flow stream, a thin shell near the surface, is monitored. This is because the strength of the electric field decays exponentially from the surface with a characteristic decay length of $d/3$, where d is the interelectrode separation.[1,5,6]

Given that 90% of the flow stream escapes examination with the ring design, we sought to develop a new sensor that has a slit configuration whereby a greater percentage of the flowing fluid can be interrogated. In addition to improving the performance of the dielectric sensor, the new device is a multifunctional unit that contains pressure and optical sensors and possesses the flexibility to add additional sensors as needed. In this paper we will describe the sensor design and its capabilities as an on-line, real-time monitor, and we will present data from the compounding of polymer/clay nanocomposites and the extrusion of polycarbonate.

II. SENSOR DESIGN[b]

The slit channel, shown in Fig. 1, with approximate dimensions of 2 mm high by 2.8 cm wide by 15 cm long, defines a constant geometry platform on which on-line sensors can be installed for the purpose of characterizing the processed material. The primary sensor in the slit channel is the dielectric sensor consisting of interdigitated electrodes that are deposited and fired onto a ceramic substrate that forms one surface of the slit. Other sensors in the current design are pressure and optical sensors situated along the axial dimension of the slit. By keeping the slit height at 2 mm or less, it is possible to fix the interelectrode separation so that the fringing electric field extends significantly into the flow stream interrogating up to 50% or more of the resin flow.

Figure 1 is a schematic of the sensor as viewed from the side and front. Two semicircular stainless steel pieces, top and bottom halves, form the cylindrical geometry of the sen-

[a]Electronic mail: abur@histogov

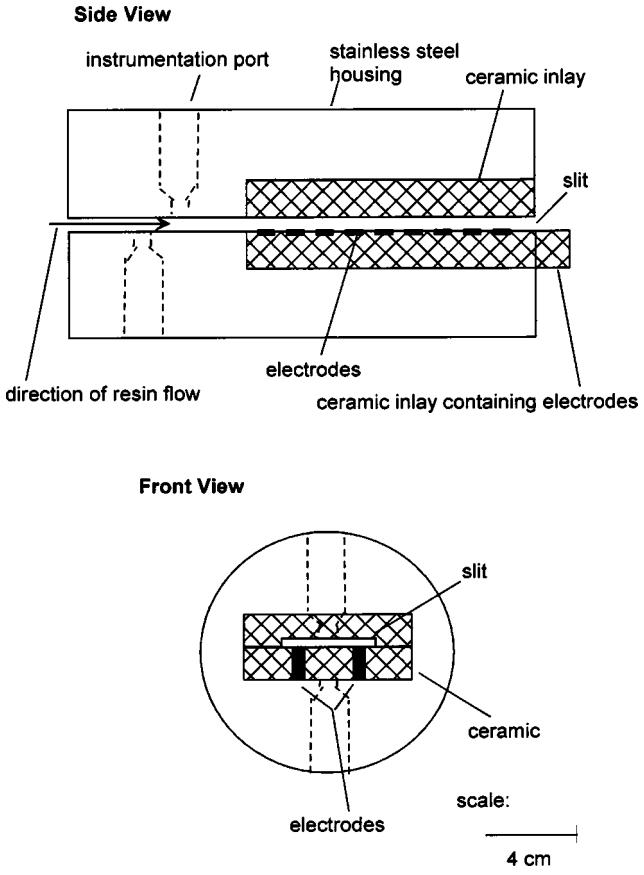

FIG. 1. The side and front views of the dielectric slit die.

sor. Its overall dimensions are 12.7 cm diameter by 15.24 cm long (5 in. diameter by 6 in. long), but the cell can be fabricated with a longer length for the purpose of adding additional instrumentation ports. Or, an additional port sector can be added in the sensor train. The sensor housing contains threaded instrumentation ports of the standard half-inch by 20 threads-per-inch type in addition to two cut-out chambers for ceramic inlays that are used for dielectric sensing. The ceramic piece on the bottom is high purity alumina onto which platinum electrodes have been deposited in an interdigitating pattern. The ceramic on top is made from machinable ceramic, has a trapezoidal cross section, and contains a cutout of the slit that is 2 mm deep by 2.8 cm wide, extending over the length of the piece, approximately 11 cm. The depth and width dimensions of the slit were machined with an accuracy of 0.012 mm. The trapezoidal cross section serves to hold the piece into place in the top half stainless steel. A heating jacket surrounds the sensor, and temperature is controlled using a thermocouple inserted into the body of the steel housing. A customized interface adapter plate positioned between the sensor and the extruder establishes the connection to the extruder. This plate contains the appropriate threaded screw holes for the specific extruder being used.

The alumina ceramic is positioned in a well that has been machined into the bottom half stainless piece and is held mechanically in place by clamping the top and bottom halves together. No epoxy or other adhesive is needed. To change ceramic substrates, the alumina block is removed from its well using the lifting bolts on the bottom of the housing to push the block out of the well. It can be replaced with electroded alumina substrates with different electrode patterns that produce fringe electric fields closer and farther from the surface and directed parallel or perpendicular to the flow. Likewise, the ceramic with the slit in the top half of the sensor can be interchanged with pieces having different slit sizes.

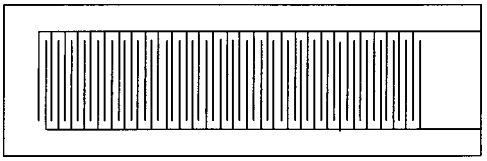

FIG. 2. The pattern of interdigitating electrodes.

A pattern of interdigitating electrodes is shown in Fig. 2. Two sets of finger electrodes are interwoven to create the sensor. Each set of fingers is connected to a lead electrode. When an alternating voltage (1 V) is applied between the electrodes, an electric field fringes between neighboring finger electrodes and extends not only through the alumina ceramic but also into the liquid media flowing above the surface. By measuring the value and phase of the resultant current and subtracting out the current through the alumina, the relative permittivity and dielectric loss of the liquid media can be determined. The measured current is resolved into its real and imaginary parts using a Stanford model SR810 lock-in amplifier. Our measurements of the complex relative permittivity, $\epsilon^* = \epsilon' - i\epsilon''$, are usually carried out over a frequency range from 500 to 10^5 Hz, or 50 to 10^5 Hz, but it is possible to operate the lock-in amplifier to frequencies as low as 0.001 Hz, although data acquisition at lower frequencies requires long times. The electronics detecting circuitry, the calibration procedure, and the software to operate the system (Chemical ElectroPhysics Proceptor Dielectric Spectrometer) are the same as have been used with the dielectric ring sensor and have been described in previous publications.[1,2]

As mentioned above, fringing electric field lines extend into both the material under investigation and into the alumina substrate. In electrical terms the two materials are in parallel. If the dielectric properties of the alumina are known, they can be ''subtracted'' from the measured total impedance, yielding the impedance of the sample material. Our experimental protocol is to carry out a cell calibration using a standard dielectric materials such as heptane and air to obtain the cell's geometrical factor [g of Eqs. (1) and (2) of Ref. 1], and to use an empty cell to measure the relative permittivity of air ϵ_{air} over the frequency and temperature range of interest. Since it is known that $\epsilon^*_{\text{air}} = 1$ and its conductance can be neglected, the dielectric properties of alumina are easily obtained and placed in a calibration table.

The slit configuration accomplishes three objectives: First, it confines the flowing liquid to a thin ribbon for which a significant fraction of its cross section is intersected by the fringing electric field lines. Second, it is the geometry of a slit die rheometer so that with knowledge of the pressure drop across the length of the slit and the flow rate, the viscosity of the material can be determined. For this purpose, a

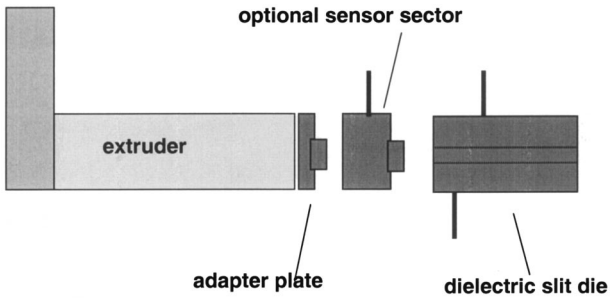

FIG. 3. The dielectric slit die and optional sensor sector.

pressure transducer is positioned upstream from the dielectric sensor and yields the value of the pressure drop along the axial length of the slit. Third, the slit is a constant geometry platform on which various sensors can be positioned.

The slit die has a flexible design that permits the addition of new sensors or instrumentation ports, or permits the interchange of sensors to different positions in the slit channel. Optional sensor port sectors, shown in Fig. 3, can be added in-line, sandwiched between the slit die and the interface plate. Ancillary sensors such as UV or infrared absorption, optical microscope, ultrasonic velocity, etc. can access the resin flow stream at this site. The optional sectors can be added or removed from service in accordance with the needs of the experiment and they can be customized to enhance sensor performance, e.g., installing optical windows for microscopy experiments.

The optics sensor is situated upstream of the dielectric sensor in the stainless steel housing of the slit die.[7,8] It consists of a bundle of seven 200 μm core optical fibers that are placed into a sleeved standard half-inch sensor bolt with a sapphire window at its end. When operating in the reflection mode, one of the fibers transmits light from the light source through a focusing lens, the sapphire window, the flowing liquid, reflects off the far stainless steel surface, and reverses its path through the material, sapphire window, and lens. The reflected light is collected by the other six fibers and is transmitted to the photomultiplier (PMT) detector. The intensity of the light source is monitored using a beamsplitter that sends a source sampling beam to another photomultiplier, as shown in Fig. 4. The ratio of the two light intensities is used to monitor the light transmission through the liquid. For the optical sensor in the reflection mode, we use a xenon arc lamp light source with a 20 nm bandpass filter centered at 570 nm. The arc lamp is chosen because it has low spatial coherence that minimizes interference phenomena. The detected light is a sum of all light that reflects from any interface along the transmission path that has a change in the index of refraction, e.g., the air/lens, air/sapphire window, sapphire window/resin, etc. The situation is depicted in Fig. 5. During processing, the interfaces of interest that will produce a change in the reflected signal are a resin/sapphire window and a resin/steel wall. Changes that occur at these interfaces will affect a change in the detected light intensity. In addition, light scattering due to filler particles attenuate the light signal. In previous work, we encountered similar geometry while carrying out an optical sensing of injection molding.[9,10]

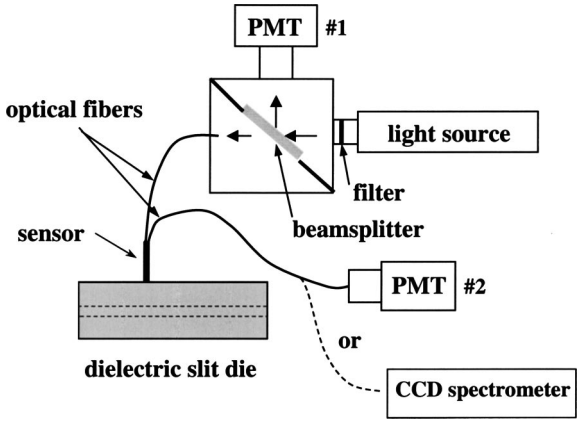

FIG. 4. The experimental setup for optical and fluorescence measurements. PMT is a photomultiplier and CCD is the charged coupled device array for acquiring spectra.

The optical sensor can also be used to monitor fluorescence from a fluorescent dye that has been doped into the polymer for the purpose of probing temperature or microstructure. The technique employs the same optical equipment that is shown in Fig. 4, except that bandpass filters, which are tuned to particular wavelengths of the fluorescence spectrum, are placed before the photomultiplier detectors and are placed in the xenon light source in order to pass light at the absorption wavelength for the dye. Alternatively, we have used a charged couple device (CCD) spectrometer to detect the entire fluorescence spectrum. Our application of fluorescence to real-time process monitoring is based on a long history of fluorescence sensor development and modeling in our laboratory. The technique is thoroughly described in several publications.[7,8,11,12] We will not present any new fluorescence data here.

Standard uncertainties for the measurements were 1 °C for temperature and 70 kPa (10 psi for pressure. The standard uncertainty in relative permittivity is 0.01 and for conductivity it is 1×10^{-10} S/m. The relative standard uncertainty in the light transmission data is 0.15%.

III. MATERIALS

To demonstrate the operation of the slit die sensor, we present real-time monitoring data for compounding nylon 12 with montmorillonite clay and for the extrusion of polycarbonate PC (PC 200.1 natural from DOW Chemical). The Nylon 12, Grilamide L16 natural, was obtained from EMS

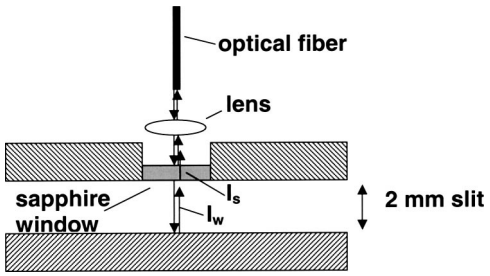

FIG. 5. Light reflections that are measured by a transmission light sensor. I_s and I_w are reflections from the sapphire window and from the wall, respectively.

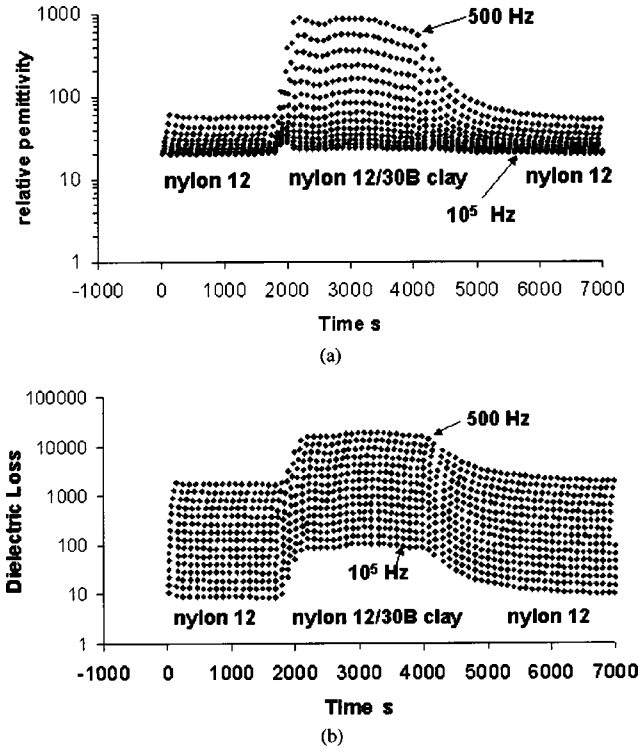

FIG. 6. (a) Relative permittivity ϵ' versus time for nylon 12 and for nylon 12/30B clay composite; (b) dielectric loss ϵ'' versus time for nylon 12 and for a nylon 12/30B clay composite.

Chemie. The clay is an organically modified clay from Southern Clay Products, Cloisite 30B. The powdered clay was compounded with the polymer at a 4% mass fraction of clay in the polymer. Compounding was carried out using an 18 mm Haake Rheocord model 9000 twin screw extruder to which the dielectric slit die was connected. These two materials were chosen to demonstrate the behavior of the dielectric sensor because their dielectric properties are at two extremes. PC has low relative permittivity and conductivity whereas nylon 12 and its clay filled composite have high values of permittivity and conductivity.

IV. RESULTS AND DATA ANALYSIS

Figure 6 shows real-time data for the extrusion of nylon 12 (neat) and for nylon 12 compounded with 4% Cloisite Clay 30B. Compounding was carried out at 195 °C. Relative permittivity, ϵ'_{meas}, and dielectric loss, ϵ''_{meas}, are plotted versus time for 15 frequencies ranging from 500 Hz to 100 kHz. At $t=400$ s, the neat polymer entered the electrode region of the dielectric sensor and was extruded for approximately 1500 s, at which time resin pellets mixed with a 4% mass fraction of clay were added to the feeder. Permittivity and conductivity began to increase as the mixture filled the slit region. After a significant transition time, the data reached a plateau value. The transition is associated with time it takes the clay/polymer mixture to completely fill the sensing region, particularly at the surface near the electrodes. At $t=4200$ s, the neat resin was again introduced and relative permittivity values returned to their original values.

The frequency dependence of relative permittivity, the dielectric dispersion, yields considerably larger change for the clay/polymer nanocomposite than for the neat polymer. This is because the introduction of the clay particles to the resin introduces ionic species that contribute to conductivity and polarization over and above that which is present in the neat resin. The resultant high conductivity creates high dielectric loss as well as electrode polarization. These factors complicate the data analysis, as we will describe below.

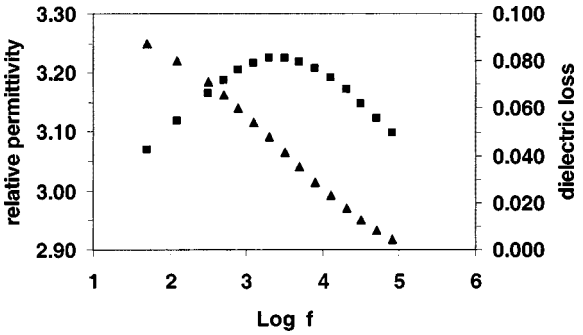

FIG. 7. Relative permittivity ϵ' (▲) and dielectric loss ϵ'' (■) for polycarbonate versus frequency at 164 °C.

Figure 7 is a plot of the relative permittivity ϵ' and dielectric loss ϵ'' of polycarbonate at 164 °C. The relaxation observed in Fig. 7 is the α relaxation associated with segmental motion of the polycarbonate molecule at temperatures above the glass transition, $T_g \approx 150\,^{\circ}\text{C}$.[13] For these data, a small but significant dc conductivity, 3.0E-9 S/m, contributed to the dielectric loss but did not create electrode polarization. The indicator of electrode polarization is an increase in ϵ' with decreasing frequency accompanied by a similar increase in ϵ'' due to dc conductivity σ_{dc}. In this case, the raw data for PC showed an increase in ϵ'' with decreasing frequency, but ϵ' remained constant. The dielectric loss data presented in Fig. 7 is that which results after subtracting out the dc conductivity contribution to ϵ'', which at any frequency ω is $\sigma_{\text{dc}}/(\epsilon_0\omega)$. Here, ϵ_0 is the permittivity of free space, 8.8549E-12 F/m. For polycarbonate, the absence of electrode polarization simplifies the data analysis in that the dc conductivity contribution to ϵ'' can be directly subtracted from the measured ϵ'' because the conductivity is electrically in parallel with the sample. When electrode polarization is significant, the data analysis is more difficult because the electrode polarization is expressed as an impedance in series with the measured sample. In general, dielectric measurements on polymer melts at processing temperatures will show electrode polarization effects. We discuss electrode polarization and its impact on the data observed for nylon 12 in the next section.

A. Analysis of dielectric measurements

When a material is subjected to an electrical field, bound charges are displaced and dipoles are oriented. Measurements made as a function of frequency of the applied electric field and temperature yield basic information about molecular dynamics, ionic conductivity, thermally activated processes, and the role of microstructure on the development of interfacial polarization.[3] The behavior is described by the complex relative permittivity $\epsilon^* = \epsilon' - i\epsilon''$. The real part of the relative permittivity ϵ' is associated with the polarization or

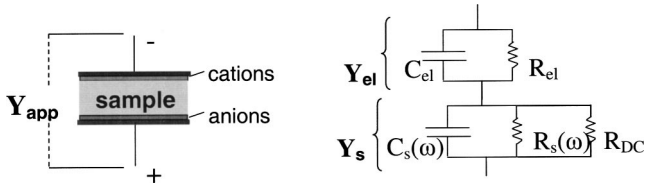

FIG. 8. Equivalent circuit used to correct for dc conductivity and electrode polarization.

capacitance of the material and the imaginary part ϵ'', the dielectric loss, is associated with its conductance.

When measuring the dielectric properties of a polymer melt at elevated processing temperatures, ion conductivity becomes a prominent feature of the behavior. This is particularly true when fillers containing ionic species are compounded with a resin matrix. In some cases the ion conductivity is so large that it overrides molecular dipolar and microstructural relaxation processes. In general, the conductivity σ can include a frequency independent component σ_{dc} associated with the drift of unbound charges and also a frequency-dependent component σ_r related to dielectric relaxation,

$$\sigma = \sigma_{dc} + \sigma_r \tag{1}$$

and

$$\epsilon'' = \frac{\sigma_{dc}}{\omega \epsilon_0} + \epsilon_r'', \tag{2}$$

where ω is radial frequency and ϵ_r'' is the relaxation frequency-dependent part of the dielectric loss and $\epsilon_r'' = \sigma_r/(\epsilon_0 \omega)$. Ionic conduction also contributes to the real part of the relative permittivity as electrode polarization or as interfacial polarization. Both of these phenomena usually occur at low frequency when ions can follow in phase with the applied electric field and accumulate at the electrode or, in a heterogeneous mixture, at the interface between components of contrasting dielectric constant. Dielectric dispersions associated with interfacial polarization are known as Maxwell–Wagner (MW) relaxations.[14] For composite materials, a distribution of permittivities and conductivities produces a distribution of relaxation times, effects that are the focus of our effort to monitor the dielectric properties of polymer composites.

A consequence of making dielectric measurements at high temperatures (needed for polymer processing) is that dissociated ions lead to dc conductivity and electrode polarization effects, both that must be taken into account in order to retrieve dielectric materials properties from the dielectric spectrum. Figure 8 depicts a sample sandwiched between electrodes that express electrode polarization due to the pileup of ions at the electrode surfaces. The situation can be described as an electrode admittance Y_{el} in series with the sample admittance Y_s. Y_{el}, consisting of a capacitance and resistance in parallel, has been called a constant phase element (CPE).[15] The admittances add to yield the apparent admittance Y_{app}, where

$$Y_{app} = G_{app} + j\omega C_{app} = \frac{Y_{el} Y_s}{Y_{el} + Y_s} \tag{3}$$

and

$$\epsilon'_{app} = \frac{C_{app}}{C_0} \quad \text{and} \quad \epsilon''_{app} = \frac{G_{app}}{\omega C_0}. \tag{4}$$

Here, G_{app} is the apparent conductance, C_{app} is the apparent capacitance, C_0 is the empty cell capacitance, and ϵ'_{app} and ϵ''_{app} are the apparent real and imaginary parts of the relative permittivity of the sample/electrode network that is measured. In practice, G_{app} and C_{app} are the components of the material/electrode impedance obtained after subtracting out the impedance of the alumina from the measured impedance of the system. Our objective is to retrieve the real and imaginary components of the sample permittivity, ϵ'_s and ϵ''_s, from the measured apparent values.

Carrying out the algebraic manipulations of the right-hand side of Eq. (3) and separating real and imaginary parts yields

$$\epsilon'_{app} = \frac{C_{app}}{C_0} = \frac{\epsilon'_s \dfrac{G_{elr}^2}{\omega^2} + \epsilon''^2_s C_{elr} + \epsilon'_s C_{elr}^2 + \epsilon'^2_s C_{elr}}{\left(\dfrac{G_{elr}}{\omega} + \epsilon''_s\right)^2 + (C_{elr} + \epsilon'_s)^2} \tag{5}$$

and

$$\epsilon''_{app} = \frac{G_{app}}{\omega C_0} = \frac{\dfrac{G_{elr}^2}{\omega^2}\epsilon''_s + \epsilon''^2_s \dfrac{G_{elr}}{\omega} + \epsilon'^2_s \dfrac{G_{elr}}{\omega} + \epsilon''_s C_{elr}^2}{\left(\dfrac{G_{elr}}{\omega} + \epsilon''_s\right)^2 + (C_{elr} + \epsilon'_s)^2}, \tag{6}$$

where G_{elr} and C_{elr} are the reduced conductance and capacitance of the electrode impedance, $G_{elr} = G_{el}/C_0$ and $C_{elr} = C_{el}/C_0$.

Our approach to solving Eqs. (5) and (6) is to assume that the dielectric dispersions are described by the Havriliak–Negami (HV) relaxation equation plus a conductivity term,[16]

$$\epsilon^* = -\frac{i\sigma}{\omega \epsilon_0} + \epsilon_\infty + \sum_j \frac{(\Delta\epsilon)_j}{[1 + (i\omega\tau_j)^{1-\delta_j}]^{\beta_j}}, \tag{7}$$

where the summation is over j relaxations, ϵ_0 is the permittivity of free space, σ is dc conductivity, ϵ_∞ is relative permittivity in the high-frequency limit, ω is radial frequency, τ_j is the relaxation time of the jth relaxation, $(\Delta\epsilon)_j$ is the strength of the jth relaxation and δ_j and β_j are the distribution of relaxation time parameters for the jth relaxation. When $\beta = 1$, Eq. (7) reduces to the Cole–Cole equation, and when $\beta = 1$ and $\alpha = 0$, the relaxation has a single relaxation time.[17] Both the Cole–Cole and HN models have been used successfully to describe dielectric behavior in polymers, solids, and in simple liquids.[3] The HN expression is a general expression that accommodates both symmetric and nonsymmetric distributions of relaxation times, whereas the Cole–Cole equation is for symmetric distributions.

In our analysis of the data, ϵ'_{app} and ϵ''_{app} were equated to the measurement by fitting Eqs. (5) and (6) to ϵ'_{meas} and ϵ''_{meas} using a nonlinear fitting routine for which the fitting parameters are those of the HN equation plus the electrode factors

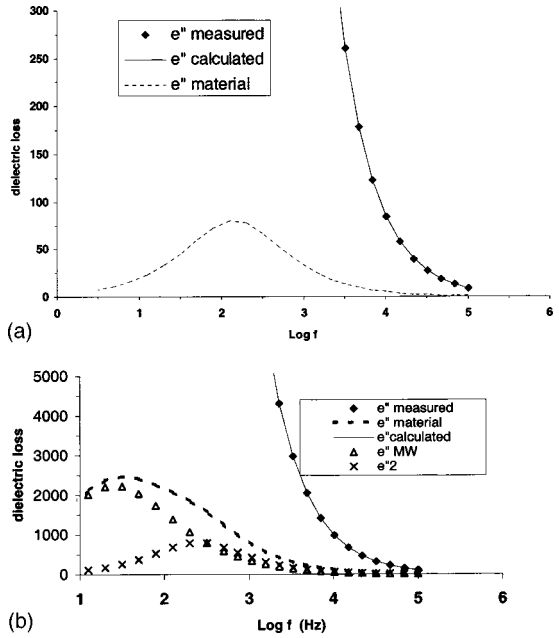

FIG. 9. Measured and calculated dielectric loss ϵ'' versus frequency for neat nylon (a) and for a nylon 12/30B clay nanocomposite (b). The dashed line is the material dielectric dispersion after dc conductivity and electrode polarization are accounted for. In (b), the MW relaxation is shown as Δ and relaxation 2 (Table I) is given as *x*.

C_{elr} and G_{elr}. That is, the real and imaginary parts of the HN equation were substituted in Eqs. (5) and (6) for ϵ_s' and ϵ_s''. To carry out the fitting process, the initial values of the fitting parameters are estimated from prior knowledge of the polymer behavior and from the appearance of the data itself. If the dielectric loss shows a peak or a shoulder on the frequency plot, we can estimate τ (or $\omega_0 = 1/\tau$). From the dependence of the measured loss at low frequencies, we can estimate σ_{dc} with the knowledge that conductivity contributes to the loss in proportion to the reciprocal of frequency. We note that the basic functional form of the HN expression is not changed during fitting; only its amplitude and position on the frequency scale. σ_{dc} and ω_0 are the most important of the fitting parameters, so that good estimates for their initial values are needed to achieve an optimum fit. Our criterion for the fit of ϵ'_{app} and $\epsilon''_{\mathrm{app}}$ to $\epsilon'_{\mathrm{meas}}$ and $\epsilon''_{\mathrm{meas}}$ is 1% difference or less between measured and calculated quantities, where a 1% criterion is chosen because it is the uncertainty in the experimental data. The fitting procedure is initiated by considering initial values of σ_{dc} and ω_0 for each dielectric relaxation that is apparent from the raw data. If the 1% criterion for a good fit is not obtained, then additional relaxation terms are added to the fitting function one at a time until the 1% criterion is satisfied.

An analysis of the dielectric loss data using Eqs. (5) and (6), yields the fits shown in Fig. 9 for the neat and clay-filled resin. After accounting for dc conductivity and electrode polarization, we obtained the dashed curve for the material dielectric properties. The optimum fitting parameters, shown in Table I, reveal that neat nylon has only one relaxation, whereas two relaxations were observed in the filled polymer. Our interpretation is that the relaxation expressed by the neat polymer at $\log f = 2.15\,(\mathrm{Hz})$ is the α relaxation associated

TABLE I. Dielectric dispersion parameters.

	Nylon 12 neat	Nylon 12/30B clay
$\log f_1$ (Hz) (MW)	···	1.41±0.02
$\log f_2$ (Hz) (α)	2.15±0.03	2.39±0.04
$\Delta\epsilon_1$ (MW)	···	6,350±200
$\Delta\epsilon_2$ (α)	202±9	1,810±300
δ_1 (MW)	···	0.236±0.02
δ_2 (α)	0.15±0.01	0.076±0.01
σ_{DC} (S/m)	4.56E-05±2E-6	4.91E-04±1E-6
β_1	···	1
β_2	1	1

with segmental dynamics of the polymer chain, and the two relaxations of the filled polymer, $\log f = 1.41\,(\mathrm{Hz})$ and $\log f = 2.395\,(\mathrm{Hz})$, are an interfacial Maxwell–Wagner (MW) relaxation and the α relaxation, respectively. The relaxation at $\log f = 1.41\,(\mathrm{Hz})$ is identified as a MW relaxation by the magnitude of its intensity $\Delta\epsilon$, 6350, a value that is indicative of ionic interfacial contributions to the polarization at the resin/clay interface and is much higher than could be produced by molecular dipoles alone.[14] The α relaxations in the neat and filled resins are different because of the impact of filler particles on the macromolecular segmental dynamics, i.e., filler particles disrupt segmental cooperativity resulting in faster α relaxation dynamics in the filled resin. We note also that σ_{dc} is approximately ten times higher for the composite than for the neat polymer due to an abundance of conducting ions that the clay contributes. The uncertainties listed in Table I were obtained from curve fitting of at least four measurements over the full frequency range. Even though σ_{dc} dominates the measured experimental value, the sensitivity of the measurement permits an accurate determination of the material's dielectric properties. The high relative permittivity of neat nylon 12, $\Delta\epsilon_2 = 202$, is the result of intermolecular cooperativity that exists in polymer melts.[18] Cooperativity is enhanced in nylons by hydrogen bonding and causes the combined contribution of multiple dipoles moments from neighboring polymer molecules to the net permittivity.

B. Optical sensing

Figure 10 shows observations of light transmission versus time for nylon 12 and its composite with 30B clay. The mixture is a 4% mass fraction of clay in the resin. Initially $(t = -1000\,\mathrm{s})$, the sensor was empty. As neat resin flowed

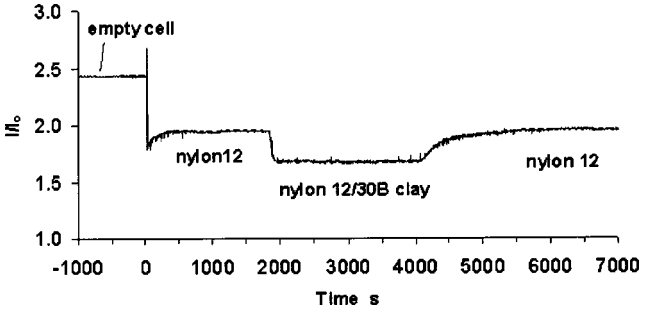

FIG. 10. Light transmission versus time for nylon 12 and a nylon 12/30B clay nanocomposite.

into the sensor field of view, an abrupt drop in light intensity occurred at $t=0$ s. This is due to a change in the reflection coefficient at two interfaces: the change from sapphire/air to sapphire/resin, and at the back wall, from steel/air to steel/resin. From $t=0$ s to $t\approx 300$ s the gradual increase in light intensity reflects the extrusion of degraded resin that occupied the extruder at the beginning of the run. A gradual cleansing of the extruder by fresh nylon resin is completed during the interval $t=0$ s to $t\approx 300$ s. At $t=1750$ s, a resin mixture containing 4% mass fraction of Cloisite 30B clay in the polymer was fed into the extruder and the resulting intensity decrease accompanies reflection coefficient changes at the interfaces and the attenuation of light due to scattering within the resin composite. At $t=4000$ s, neat nylon 12 was fed into the flow stream and the light intensity slowly returned to the original level as the composite material was replaced by the neat resin. The transition from the nylon/30B composite to neat nylon 12 took approximately 1500 s.

The objective of measuring light transmission data is to obtain an attenuation coefficient for the processed resin. If we assume that the reflection coefficients at the sapphire window and the steel wall are the same for both the neat resin and the 4% filled resin, then the light attenuation is due to the scattering of filler particles. If we describe attenuation by Beer's law, $I=I_0e^{-\beta x}$, where I is light intensity, β is the attenuation coefficient, and x is distance, then $\beta=0.39$ cm^{-1} for the filled resin intensity reduction in Fig. 10. A more detailed discussion of the optics sensor is contained in previously published papers.[9,10]

The same transition times are seen in the dielectric data, where the change from neat to composite and back to neat resin is reflected in the relative permittivity and conductivity data of Fig. 6. The lengthy transition times are due to the flow pattern by which new resin replaces old in the slit. When added to the extruder, the new resin does not immediately replace old resin, but rather, follows laminar flow streams of highest velocity that are at the center of the slit. In time, the boundary between new and old resin moves toward the surface and the sensitive region of the dielectric sensor, at which time the slit becomes completely full.

Figure 11 shows the corresponding pressure signal as a function of time. Steady-state conditions prevail after the transitions are complete. The calculation of resin apparent viscosity using slit die rheology yielded values of 139 and 169 Pa s for the neat and filled nylon 12, respectively.[19] The relative uncertainty in the apparent viscosity values is 8%.

In summary, the dielectric slit die was specifically designed to monitor polymer nanocomposites compounding. A multiplicity of sensors permits the characterization of the compounded product from different perspectives. We showed that the dielectric response of a polymer melt displays electrode polarization and dc conductivity, effects that must be taken in account when analyzing the data in order to retrieve material dielectric relaxations. One can expect that Maxwell–Wagner relaxations will be present in polymer composites containing inorganic filler.

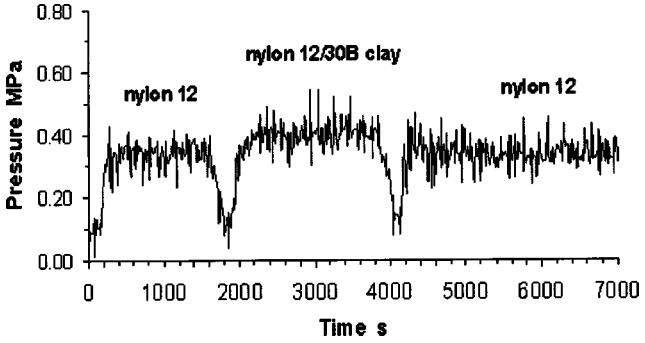

FIG. 11. Pressure versus time for nylon 12 and a nylon 12/30B nanocomposite.

The uniqueness of this instrument is highlighted by the fact that there are very little dielectric data in the literature for polymer melts that we can use as a reference. Most researchers have avoided working on polymer melts because operating a static dielectric cell at melt processing temperatures will cause polymer degradation in a matter of minutes and potentially cause damage to the instrument. The data that we present here represent investigations into an area of parameter space that has not been explored before.

[b]Identification of a commercial product is made only to facilitate experimental reproducibility and to describe adequately the experimental procedure. In no case does it imply endorsement by NIST or imply that it is necessarily the best product for the experiment.

[1] A. J. Bur, S. C. Roth, and M. McBrearty, Rev. Sci. Instrum. **73**, 2097 (2002).
[2] S. Perusich and M. McBrearty, Polym. Eng. Sci. **40**, 214 (2000).
[3] *Dielectric Spectroscopy of Polymeric Materials: Fundamentals and Applications*, edited by J. P. Runt and J. J. Fitzgerald (American Chemical Society, Washington, DC, 1997).
[4] A. Boersma and J. van Turnhout, Polymer **40**, 5023 (1999).
[5] M. C. Zaretsky, L. Mouayad, and J. R. Melcher, IEEE Trans. Electr. Insul. **23**, 897 (1988).
[6] M. C. Zaretsky, P. Li, and J. R. Melcher, IEEE Trans. Electr. Insul. **24**, 1159 (1989).
[7] A. J. Bur, M. G. Vangel, and S. C. Roth, Polym. Eng. Sci. **41**, 1380 (2001).
[8] K. B. Migler and A. J. Bur, Polym. Eng. Sci. **38**, 213 (1998).
[9] C. L. Thomas and A. J. Bur, Polym. Eng. Sci. **39**, 1619 (1999).
[10] C. L. Thomas and A. J. Bur, Polym. Eng. Sci. **39**, 1291 (1999).
[11] A. J. Bur and C. L. Thomas, Polym. Eng. Sci. **37**, 1430 (1997).
[12] A. J. Bur, M. G. Vangel, and S. Roth, Appl. Spectrosc. **56**, 174 (2002).
[13] G. J. Pratt and M. J. A. Smith, Polym. Int. **40**, 239 (1996).
[14] R. W. Sillars, J. Inst. Electr. Eng. **80**, 378 (1937).
[15] F. Pizzitutti and F. Bruni, Rev. Sci. Instrum. **72**, 2502 (2001).
[16] S. Havriliak and S. Negami, J. Polym. Sci., Part C: Polym. Symp. **14**, 99 (1966).
[17] R. H. Cole, J. Chem. Phys. **23**, 493 (1955).
[18] K. L. Ngai, J. Chem. Phys. **109**, 6982 (1998).
[19] P. W. Springer, R. S. Brodkey, and R. E. Lynn, Polym. Eng. Sci. **15**, 583 (1975).